



Research paper

Design and analysis of a metamorphic mechanism cell for multistage orderly deployable/retractable mechanism



Kun Xu^a, Long Li^a, Shaoping Bai^b, Qiaolong Yang^c, Xilun Ding^{a,*}

^a School of Mechanical Engineering and Automation, Beihang University, 37 Xueyuan Road, Beijing, 100191, China

^b Department of Mechanical and Manufacturing Engineering, Aalborg University, Fibigerstraede 16, Aalborg 9000, Denmark

^c Beijing Institute of Spacecraft System Engineering, 102 Youyi Road, Beijing, 100094, China

ARTICLE INFO

Article history:

Received 26 October 2016

Revised 4 January 2017

Accepted 31 January 2017

Keywords:

Variable kinematic joint

Friction self-locking

Variable topology mechanism

Metamorphic mechanism

ABSTRACT

Normal kinematic joint can be transformed to variable kinematic joint(VKJ), which refers to a kinematic joint that is capable of topological variation in a mechanism, by utilizing effect of friction and self-locking. In this paper a metamorphic mechanism cell which can realize deploying, self-locking, unlocking, retracting and interlocking with other cells, is designed by incorporating VKJs. Self-locking margin is proposed to estimate the self-locking capability. The variable topology configurations of this cell are presented and the mobility of this cell is analyzed. With the new metamorphic cell, a cable-driven telescopic model with 3 tubes is built, and its motion simulations are conducted to verify the design method. The results demonstrate that the impact in transformation is mitigated and multistage orderly deployable/retractable mechanisms can be built by this method.

© 2017 Elsevier Ltd. All rights reserved.

1. Introduction

A class of mechanisms whose topology configurations are changeable to meet different task requirements is called metamorphic mechanism [1], also known as the mechanism with variable topologies(MVTs) [2,3]. The mobility of this class of mechanisms is accordingly changed with their configuration variation. These mechanisms are generally functioned by the variable kinematic joints(VKJs) whose types and/or representative orientations are changeable during a cycle of motion [4,5]. Several types of these joints were illustrated by Yan and Kuo [5]. Gan et al. [6] presented the reconfigurable Hook (rT) joint and two types of metamorphic parallel mechanisms assembled with this rT joint.

The MVTs or metamorphic mechanisms have been widely studied. Matrix representation [7] and topological graph [8–10] are two main methods used to represent the topological configuration. Pucheta et al. [11] analyzed the topological configuration using the graph theory method and their synthesis method has been successfully applied to design a family of low-voltage circuit breakers. Li and Dai [12] presented a method of structure composition of single-driven metamorphic mechanisms based on augmented Assur groups. Balli and Chand [13,14] proposed a method for the synthesis of five-bar motion with variable topology and an analytical method of synthesis of a planar seven-link mechanism with variable topology.

The realization of MVTs can depend on the friction effects which change the motion of the kinematic joint. The frictional force causes self-locking which leads to change of topology of a mechanism. Oledzki [15] described the classification of self-locking drives and proposed a physical model of a self-locking kinematic pair. Leonesio and Bianchi [16] proposed a definition of self-locking for multi-DoF(Degree of Freedom) mechanisms and presented an algorithm for computing the

* Corresponding author.

E-mail address: xlding@buaa.edu.cn (X. Ding).

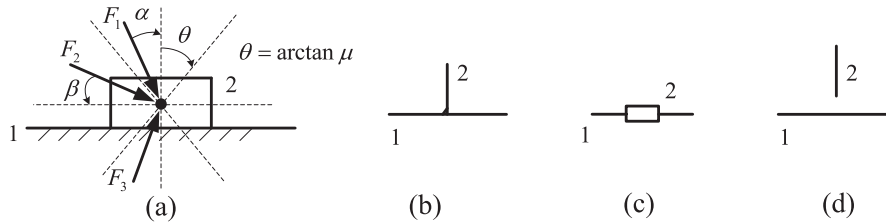


Fig. 1. Friction models of planar pair under different driving, (a) planar pair, (b) equivalent fixed pair, (c) equivalent prismatic pair, (d) equivalent separated pair.

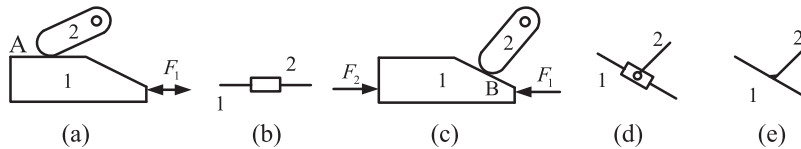


Fig. 2. Friction models of cam pair under different conditions, (a) cam pair coupled at line A, (b) equivalent prismatic pair, (c) cam pair coupled at line B, (d) equivalent prismatic pair and revolute pair, (e) equivalent fixed pair.

geometrical locus that corresponds to a specific self-locking configuration. Xu and Ding [17,18] studied walking robot as metamorphic mechanisms by assuming the constraints between supporting foot and ground with different hinges. Ding and Li [19] developed a deployable/retractable mechanism using the joint friction effect.

Deployable/retractable mechanisms can be used in aerospace field. Relevant examples include the extendable retractable telescopic mast [20], the deployable optical telescope [21], the CFRP Boom and the DLR Boom [22], the Sula Boom for the Cibola Flight Experiment Satellite [23], and the FAST mast for the international Space Station [24]. The MVTs/metamorphic mechanisms can be used to construct multistage deployable mechanisms and new designs can be proposed.

In this paper, several variable kinematic joints are analyzed with consideration of effects of friction and the driving forces. By making of variable kinematic joints, one metamorphic mechanism cell which can be self-locking and inter-locking with other cells is designed. Self-locking margin is proposed to assess the self-locking capability, upon which the mobility of this cell is analyzed. Moreover the expansion designs of the metamorphic mechanism cell in parallel and in serial are described. A design example of cable driven mechanism which can be orderly deployable/retractable is presented with simulations to demonstrate the design method.

2. Metamorphic mechanism cell design for self-locking, interlocking and unlocking

2.1. Specific variable kinematic joints using friction effect

Equivalent kinematic pair is often used in mechanism analysis [25,26]. Using equivalent kinematic pair friction effect and driving direction can make a normal joint transformed to a variable kinematic joint. As shown in Fig. 1(a), body 1 and body 2 form a planar pair. If the driving force F_1 was applied in friction lock area (inside the friction cone), there are no relative movements between body 1 and body 2. The equivalent joint is shown in Fig. 1(b). When driving force F_2 was applied in sliding area, body 2 could slide on body 1, the equivalent joint is a prismatic pair, shown as Fig. 1(c). If the driving force F_3 was applied in separating area, body 2 would move away from 1, the equivalent joint is a separated pair, shown as Fig. 1(d).

Similarly, considering effects of friction, specific cam pair can be equivalent to variable kinematic joints. A cam pair composed of bodies 1 and 2 is shown in Fig. 2. The contact surface is represented by two lines: line A and line B. When bodies 1 and 2 are coupled at line A as shown in Fig. 2(a), they can slide on each other under the driving force F_1 . Its equivalent joint is a prismatic pair as shown in Fig. 2(b). As shown in Fig. 2(c), bodies 1 and 2 are coupled at line B. If body 1 is driven by F_1 , they can slide on each other and body 2 can rotate by its axis. So the equivalent joint is a combination of a prismatic pair and a revolute pair, as shown in Fig. 2(d). When body 1 is driven by F_2 and no friction lock is satisfied, the equivalent joint is the same as Fig. 2(d). When body 1 is driven by F_2 and friction lock is satisfied, its equivalent joint is a fixed pair, as shown in Fig. 2(e).

A wedge planar pair composed by bodies 1 and 2 is shown in Fig. 3(a). If driving force F_1 is applied, the relationship between bodies 1 and 2 can be seen as a prismatic pair as shown in Fig. 3(b) without considering the friction. When the friction effects are taken into account, the relationship between bodies 1 and 2 will vary. The equivalent joint can be seen as a fixed pair as shown in Fig. 3(c) while friction lock is satisfied. Under this condition if driving force F_2 is applied as shown in Fig. 3(a), its equivalent joint transforms into a prismatic pair as same as the one without friction.

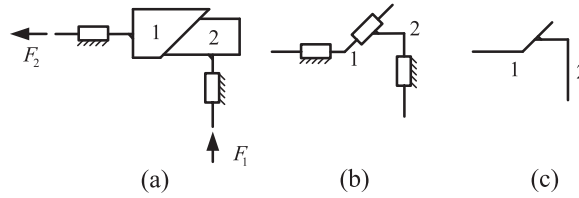


Fig. 3. Friction model of wedge surface pair under different conditions, (a) wedge planar pair, (b) equivalent prismatic pair, (c) equivalent fixed pair.

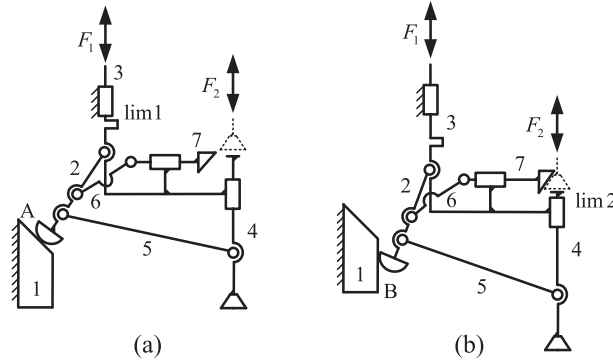


Fig. 4. Metamorphic mechanism cell diagrams, (a) coupled at line A, (b) coupled at line B.

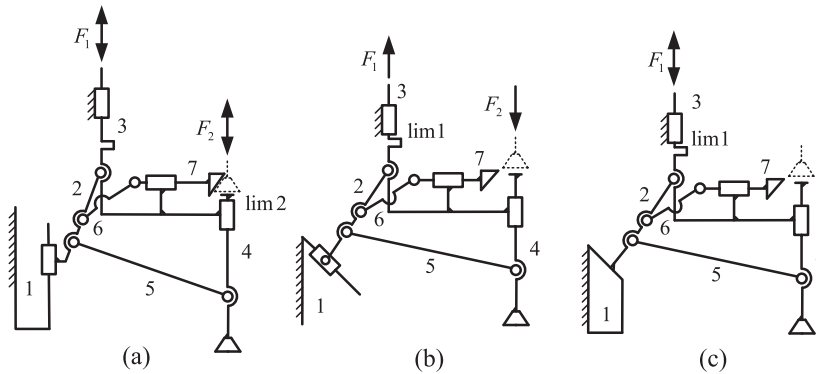


Fig. 5. Equivalent mechanisms of metamorphic mechanism cell in different stage, (a) equivalent mechanism in deploying and retracting stages, (b) equivalent mechanism in locking and unlocking stages, (c) equivalent mechanism in locked stage.

2.2. Metamorphic mechanism cell

From the above three instances, it is seen that a kinematic joint can be transformed to a variable kinematic joint depending on driving forces. A new metamorphic mechanism cell using cam pair and wedge surface pair is designed, as shown in Fig. 4. The mechanism cell can realize self-locking, inter-locking and unlocking. The motion of the metamorphic mechanism cell can be divided into 5 stages: deploying stage, locking stage, locked stage, unlocking stage and retracting stage. In locking stage, locked stage and unlocking stage, body 1 and body 2 contact on the slope plane, mechanism cell has the same diagram as shown in Fig. 4(a). In locked stage the limit, namely lim1 between body 1 and link 3, is in action. In deploying stage and retracting stage, body 1 and body 2 contact on the vertical plane, mechanism cell diagram is shown in Fig. 4(b). In retracting stage the limit, called lim2 between link 3 and link 4, is in action. Although the diagrams of mechanism in different stage are the same, the configurations (or equivalent mechanisms) are different. Configuration of deploying stage is shown in Fig. 5(a). As in retracting stage the motion is inverse to the motion in deploying stage, configuration remains the same. Under this configuration, driving force can be applied as F_1 or F_2 . When the direction of driving force is upward, the mechanism starts to deploy. Otherwise the mechanism is retracting. Configuration of locking stage under driving force F_1 is shown in Fig. 5(b). In unlocking stage the motion is inverse to the motion in locking stage under driving force F_2 , and they have the same configuration. In the locked stage body 1 and body 2 are locked by friction, they can be seen as fixed together. Equivalent mechanism of locked stage is shown in Fig. 5(c). Driving force F_1 can not actuate the mechanism because of the limit lim1 and the friction effect.

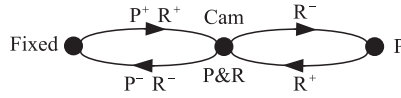


Fig. 6. Diagram of the variable kinematic joint between bodies 1 and 2.

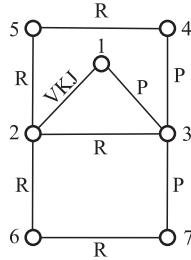


Fig. 7. Graph topology representation of the metamorphic mechanism cell.

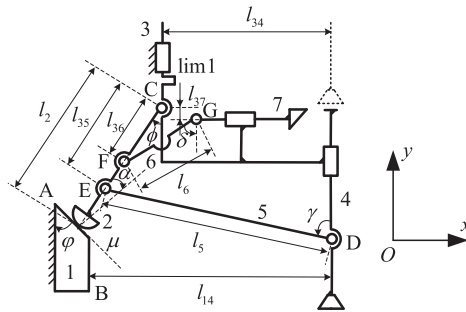


Fig. 8. Self-locking and unlocking part of the metamorphic mechanism cell.

In the metamorphic mechanism cell the joint between bodies 1 and 2 is kinematically variable. The transformation of this joint is shown in Fig. 6. Each vertex denotes topology state of the variable joint and the ordered arc represents the transformation between two topology states. In the figure P, R, Cam and Fixed stand for prismatic, revolute, cam and fixed pair respectively. Three nodes P, Cam and Fixed are corresponding to Fig. 5(a), 5(b) and 5(c) respectively. The arrow shows transformation direction, while the right superscript of the notation symbolizes the motion operation, in which “+” indicates adding motion and “-” means releasing motion. The graph representation indicates relationships among parts of a mechanism. Fig. 7 shows the relationships among parts of the metamorphic mechanism cell.

3. Self-locking and unlocking conditions analysis

The variable kinematics joints studied in this paper utilize friction effects and driving directions to realize transformation of different motions. Friction effects and driving directions play a decisive role of self-locking and unlocking of the joint. The self-locking condition will not be satisfied, due to the external disturbance force on the joint. The self-locking capability of joint to resist the external disturbance is named self-locking stability. In order to quantify and calculate this self-locking stability, self-locking margin is proposed and defined as,

$$M_{lock} = \frac{\theta - \alpha}{\theta} = 1 - \frac{\alpha}{\theta} \tag{1}$$

where $\theta = \arctan \mu$ is the friction angle with μ being the coefficient of friction of joint, α is the angle between driving direction and normal pressure direction, as shown in Fig. 1(a).

When $M_{lock} = 1$, this means $\alpha = 0$, the driving direction coincides with normal pressure direction. The self-locking capability of the joint reaches maximum. As a result, the locking condition is most stable.

When $M_{lock} = 0$, this means $\alpha = \theta$, the driving direction and the moving direction make an angle identical to the friction angle. The joint is in critical self-locking/unlocking condition.

When $M_{lock} < 0$, this means $\alpha > \theta$, the self-locking is invalid. The driving force moves the link, either to translate or rotate.

As shown in Fig. 8, the self-locking margin of the mechanism cell can be obtain by

$$M_{lock} = 1 - \frac{\alpha}{\theta} = 1 - \frac{\pi/2 - \phi - \varphi}{\arctan \mu} \tag{2}$$

Eq. (2) shows that the self-locking margin of the mechanism cell is determined by the angle φ of the slop of the body 1, the angle ϕ between link 2 and link 3 and the friction coefficient μ between body 1 and link 2. Under self-locking condition, $0 < M_{lock} \leq 1$, hence Eq. (2) can be modified as

$$0 < 1 - \frac{\pi/2 - \phi - \varphi}{\arctan \mu} \leq 1 \tag{3}$$

The relationship among angles φ , ϕ and friction coefficient μ can be obtained as

$$\pi/2 - \arctan \mu \leq \varphi + \phi < \pi/2 \tag{4}$$

Eq. (4) can be modified as

$$\mu > \cot(\varphi + \phi) \tag{5}$$

Eqs. (2) and (5) can be used to analyze and evaluate the self-locking capability, and guide the design of the mechanism cell.

Unlock driving force is applied on link 4, which is further transferred via link 5 to link 2. During unlocking stage the unlocking torque must stronger than the resisting torque from friction effect. In unlocking there are two situations: one is only unlocking force F_2 applied on link 4, the other is force F_1 applied on link 3 besides F_2 applied on link 4. Both situations will be discussed respectively.

When only unlocking force F_2 applied on link 4, the torque generated by two-force bar 5 reference to the revolution joint C can be obtained as

$$\tau_u = F_2 \cos \gamma \sin(\pi - \gamma - \phi) l_{35} \tag{6}$$

where l_{35} is the length between the axes of revolute joints E and F.

The torque generated by normal force between bodies 1 and 2 reference to the revolute joint C can be obtained as

$$\tau_n = F_2 \cos \gamma \cos(\pi - \gamma - \phi) \sin(\pi/2 - \varphi - \phi) l_2 \tag{7}$$

where l_2 is the length of link 2.

The resistance torque generated by friction between bodies 1 and 2 reference to the revolute joint C can be obtained as

$$\tau_f = \mu F_2 \cos \gamma \cos(\pi - \gamma - \phi) l_2 \tag{8}$$

The mechanism can be unlocked while unlock torque and resistance torque satisfies

$$\tau_u + \tau_n > \tau_f \tag{9}$$

The unlocking condition can be expressed as

$$u < \frac{\sin(\gamma + \phi) l_{35} - \cos(\gamma + \phi) \cos(\varphi + \phi) l_2}{-\cos(\gamma + \phi) l_2} \tag{10}$$

When there is another force F_1 applied on link 3, the torque generated by two-force bar 5 is obtained by Eq. (6).

The torque generated by normal force between bodies 1 and 2 reference to the revolute joint C can be obtained as

$$\tau_n = F_2 \cos \gamma \cos(\pi - \gamma - \phi) \sin(\pi/2 - \varphi - \phi) l_2 + F_1 \cos \phi \sin(\pi/2 - \varphi - \phi) l_2 \tag{11}$$

The resistance torque generated by friction is changed. It can be obtained as,

$$\tau_f = \mu [F_2 \cos \gamma \cos(\pi - \gamma - \phi) + F_1 \cos \phi \cos(\pi/2 - \varphi - \phi)] l_2 \tag{12}$$

According to Eq. (9), the unlocking condition can be obtained as

$$u < \frac{F_2 \cos \gamma \sin(\gamma + \phi) l_{35} - F_2 \cos \gamma \cos(\gamma + \phi) \cos(\varphi + \phi) l_2 + F_1 \cos \phi \cos(\varphi + \phi) l_2}{F_2 \cos \gamma \cos(\gamma + \phi) l_2 + F_1 \cos \phi \sin(\varphi + \phi) l_2} \tag{13}$$

While F_1 equals to zero, Eq. (13) will degrade to Eq. (10).

Eq. (13) can be modified as

$$F_2 > \frac{\mu F_1 \cos \phi \sin(\varphi + \phi) l_2 - F_1 \cos \phi \cos(\varphi + \phi) l_2}{\cos \gamma \sin(\gamma + \phi) l_{35} - \cos \gamma \cos(\gamma + \phi) \cos(\varphi + \phi) l_2 - \mu \cos \gamma \cos(\gamma + \phi) l_2} \tag{14}$$

4. Mobility analysis of the metamorphic mechanism cell

The mobility of mechanism is calculated as [1]

$$m = d(n - g - 1) + \sum_{i=1}^g f_i \tag{15}$$

where n is the number of links, g is the number of working joints, and f_i is the degrees of freedom of joint i . Parameter d is the order of the screw system applied in the mechanism.

4.1. Mobility of the equivalent mechanism in deploying and retracting stages

Consider the equivalent mechanism in Fig. 5(a) and the topology configuration in Fig. 7, there are 3 independent loops in the mechanism. Two of them are 3-order loops and one is 2-order loop. So the mobility is given as follows

$$m = 9 - 2 \times 3 - 2 = 1.$$

This means in deploying/retracting stage the metamorphic mechanism cell has one DoF. In deploying/retracting stage,

$$v_D = v_C \quad (16)$$

where v_D is the velocity of joint D, also the velocity of link 4, and v_C is the velocity of joint C, also the velocity of link 3.

4.2. Mobility of the equivalent mechanism in locking and unlocking stage

Consider the equivalent mechanism in Fig. 5(b), the mobility is given by Eq. (15) as follows

$$m = 3 \times (8 - 10 - 1) + 10 = 1.$$

This means in locking/unlocking stage the metamorphic mechanism cell has 1 DoF. According to the structure in Fig. 5(b) and Fig. 8, the following equations can be obtained,

$$\begin{cases} x_{12} - x_{1A} = -(y_{12} - y_{1A}) \tan \varphi \\ P_{12} = P_C + (P_E - P_C)l_2/l_{35} \\ P_{12} = P_C + (P_F - P_C)l_2/l_{36} \\ \|P_{12} - P_C\| = l_2 \\ \|P_F - P_C\| = l_{36} \\ \|P_C - P_E\| = l_{35} \\ \|P_E - P_D\| = l_5 \end{cases} \quad (17)$$

where $P_{12} = (x_{12}, y_{12})$ is the coordinate of equivalent revolute joint axis between bodies 1 and 2, $P_{1A} = (x_{1A}, y_{1A})$ is an arbitrary point in the direction line A of the joint between bodies 1 and 2, P_C , P_D , P_E , and P_F are the coordinates of the relevant joints respectively.

Moreover, according to the geometric constrains in Fig. 8, the relationship among v_C , v_D and v_{12} can be obtained

$$\begin{cases} v_C = v_{12} \cos \varphi - v_{12} \sin \varphi \tan \phi \\ v_D = v_C + (l_{35}/l_2)v_{12} \sin \varphi \tan \phi + (l_{35}/l_2)v_{12} \sin \varphi \tan \gamma \\ v_G^x = (l_{35}/l_2)v_{12} \sin \varphi - (l_{35}/l_2)v_{12} \cos \varphi \cot \delta \\ v_G^y = v_C \end{cases} \quad (18)$$

where v_{12} is the velocity of the equivalent revolute joint axis between bodies 1 and 2.

The relationship between v_C and v_D can be obtained from Eq. (18),

$$\frac{v_D}{v_C} = 1 + \frac{l_{35}}{l_2} \frac{\sin \varphi (\tan \phi + \tan \gamma)}{\cos \varphi - \sin \varphi \tan \phi} \quad (19)$$

4.3. Mobility of the equivalent mechanism in locked stage

The mobility of the equivalent mechanism in Fig. 5(c) is given as follows

$$m = 3 \times (5 - 6 - 1) + 6 = 0.$$

This is nothing surprising, as the whole mechanism is locked.

According to above mobility analysis of the metamorphic mechanism cell, the mechanism cell has one DoF when it is moving. When mechanism is locked it has no DoF. So the mechanism cell can be actuated by only one driver.

5. Expanding design based on the mechanism cell

5.1. Parallel expansion

The metamorphic mechanism cell can be used to build large scale orderly deployable/retractable mechanisms by two extensions: serial and parallel connection. The serial connection can extend the length of the mechanism and the parallel connection can improve the mechanical behavior of the mechanism. Fig. 9 shows n metamorphic mechanism cells bonded together by parallel connection. Links 1, 3 and 4 of each metamorphic mechanism cell are fixed together respectively, which ensures the synchronized movement of each cell. Fig. 10 shows the structure of parallel expansion with 2 metamorphic

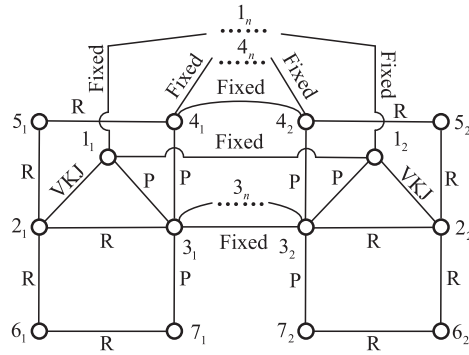


Fig. 9. The graph representation of parallel extension with n metamorphic cells.

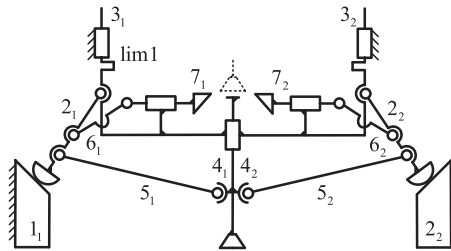


Fig. 10. Diagram of parallel extension with 2 metamorphic cells.

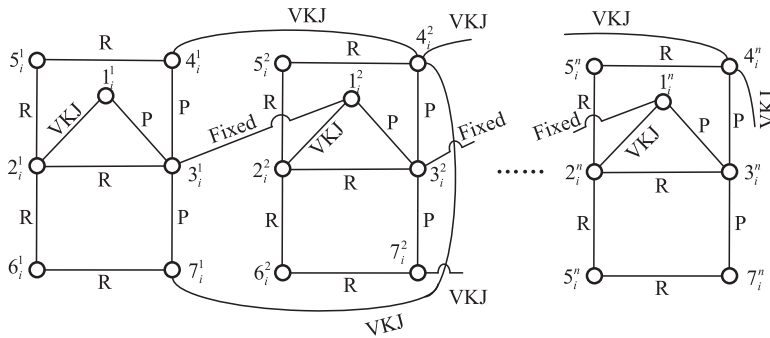


Fig. 11. The graph representation of serial extension with n metamorphic cells.

mechanism cells. According to graph representation in Fig. 9, more cells can be used to form parallel expansion. These parallel expansions of the metamorphic mechanism cells have the same kinematics with one mechanism cell. Thus the DoF of parallel expansions is equal to 1 when the parallel expansions are in deploying/retracting stage and locking/unlocking stage. The parallel expansions have 0 DOF when they are locked.

In parallel expansion, the self-locking margin can be obtained by

$$M_{lock} = \max(M_1, M_2, \dots, M_n) \tag{20}$$

where M_n is the self-locking margin of the n-th cell. This means the self-locking condition is determined by the most stable metamorphic mechanism cell.

5.2. Serial extension

In parallel expansions, all metamorphic mechanism cells have synchronized motion. This type of combination can enhance the mechanical behavior of the equipment but can not realize large dimension deploying. To achieve large scale extension the metamorphic mechanism cells can be connected in series. The graph topology representation is shown in Fig. 11. The right superscript denotes the order of the structure and the right subscript denotes the number of the cell in specific order. The structures of serial extension with n metamorphic mechanism cells under different stages are shown in Fig. 12.

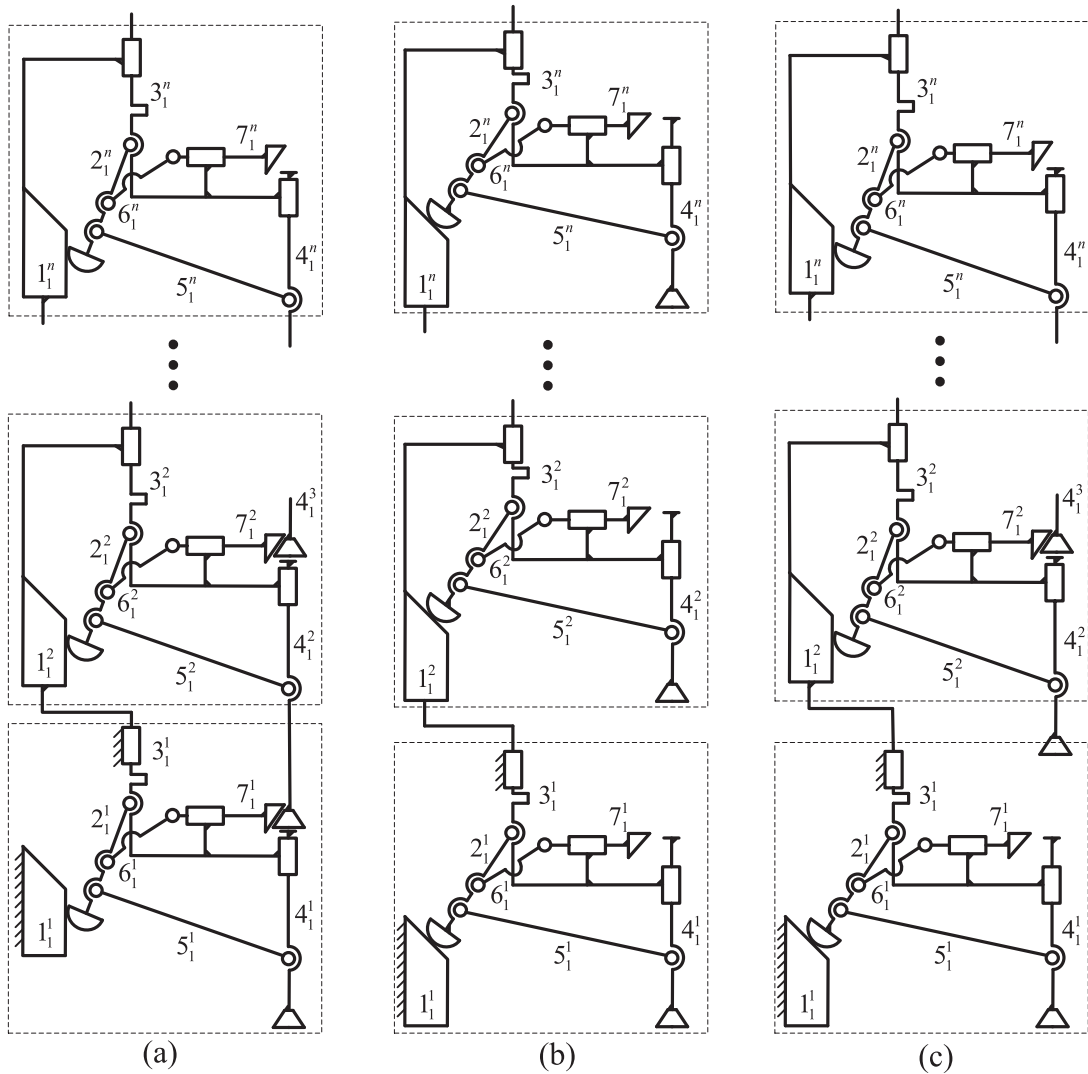


Fig. 12. The diagram of serial extension with n metamorphic cells, (a) fully retracting stage, (b) fully deploying stage, (c) intermediate stage.

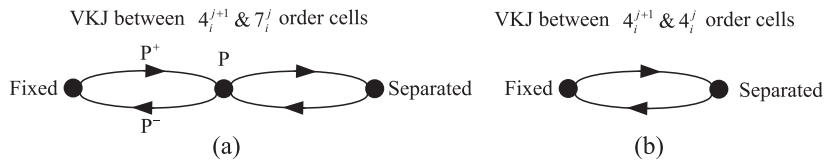


Fig. 13. Transformation of VKJ between jth and (j + 1)th order cells.

When the serial extension is in fully retracting condition, all adjacent cells are interlocked through the restriction between part 4_i^{j+1} and part 7_j^j , as shown in Fig. 12(a). All cells are fixed except the first one. So the serial extension has 1 DoF and the first cell can deploy. When the first cell deploys into locking stage, the VKJ between part 4_i^2 and part 7_i^1 transfers to prismatic pair. The motion of this prismatic pair depends on the movement of the first cell. So the whole system also has 1 DoF. When the first cell realizes full deploying and self-locking, the VKJs between first cell and second cell are transformed to separated pairs. The combination of the second to n-th cells will repeat the deployment process like the first cell until the n-th cell completes full deploying and self-locking, as shown in Fig. 12(b). The retracting process has inverse procedures of deploying process. The transformation of VKJs between adjacent metamorphic mechanism cells is shown in Fig. 13.

In serial expansion, the self-locking margin can be obtained by

$$M_{lock} = \min(M^1, M^2, \dots, M^n) \tag{21}$$

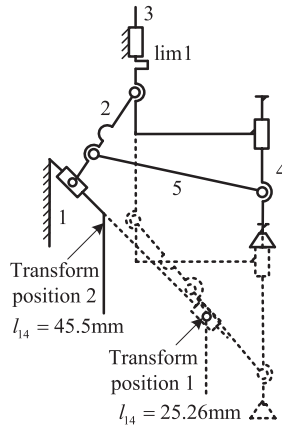


Fig. 14. Transform position while $l_{14} = 45.5 \text{ mm}$ & $l_{14} = 25.26 \text{ mm}$.

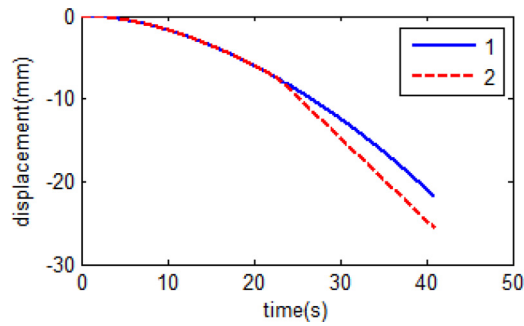


Fig. 15. Displacement of link 3 when unlocking by link 4, $v_D = -1 \text{ mm/s}$.

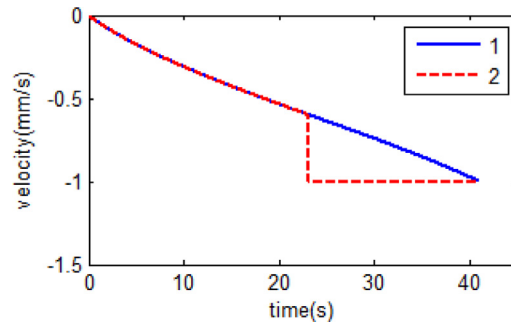


Fig. 16. Velocity of link 3 when unlocking by link 4, $v_D = -1 \text{ mm/s}$.

where M^n is the self-locking margin of the n-th unit. This means the self-locking condition is determined by the weakest metamorphic mechanism cell.

If each order unit has m cells, the serial extension of these units has same deploying/retracting process as above mentioned because the cells in the same order unit have identical motion.

6. Implement design and simulation

6.1. Simulation of metamorphic cell

Kinematics simulation has been conducted to determine the parameters of the metamorphic cell. Assuming the parameters $\varphi = 45^\circ$, $l_2 = 18.5 \text{ mm}$, $l_{35} = l_{36} = 12 \text{ mm}$, $l_5 = 50 \text{ mm}$, $l_{34} = 36 \text{ mm}$, and $l_6 = 25 \text{ mm}$, respectively. In Eq. (17), taking

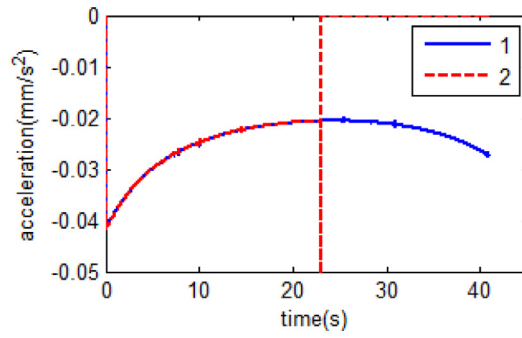
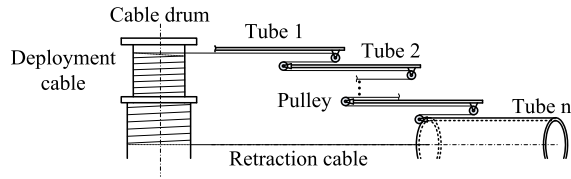
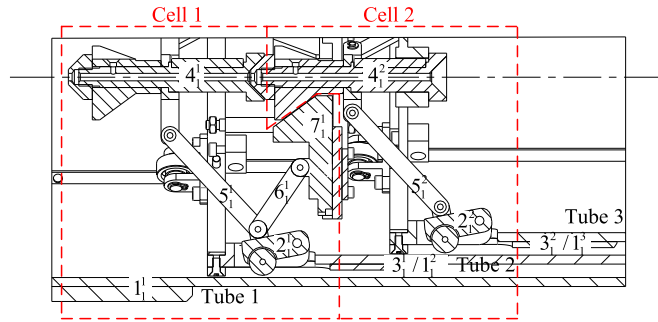


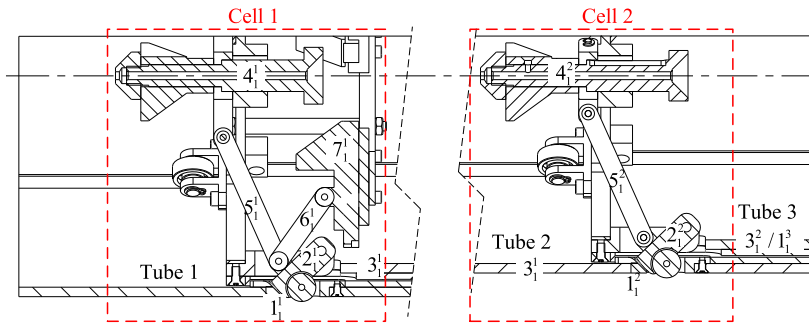
Fig. 17. Acceleration of link 3 when unlocking by link 4, $v_D = -1$ mm/s.



(a) Drive system with cables and pulleys



(b) Fully retracted stage



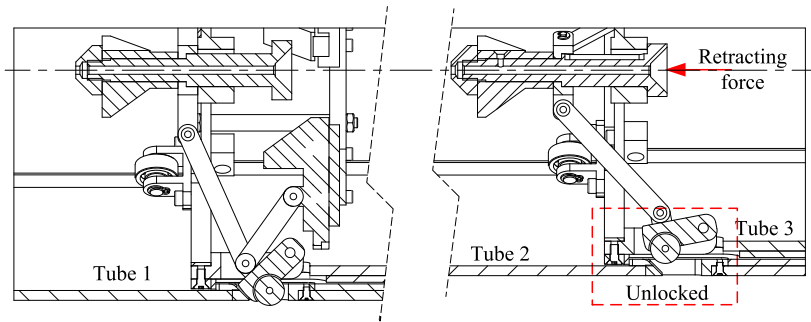
(c) Fully deployed stage

Fig. 18. Implement design of the orderly deployable/retractable mechanism.

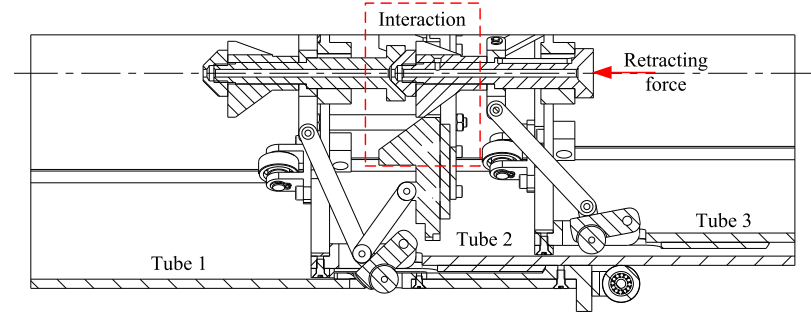
$P_{1A} = (-36, -18.5\sqrt{2})$, the following is obtained,

$$\begin{cases} y_{12} = \frac{y_C - \sqrt{-y_C^2 - 37\sqrt{2}y_C - 18.5\sqrt{2}}}{2} \\ y_D = \frac{6.5y_C + 12y_{12} - \sqrt{(50 \times 18.5)^2 - (12y_{12} + 666 + 222\sqrt{2})^2}}{18.5} \end{cases} \quad (22)$$

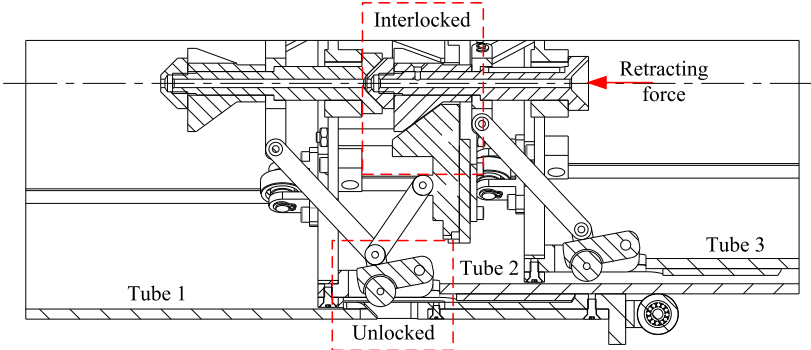
where y_C is the y-axis coordinate of joint C between links 2 and 3, y_{12} is the y-axis coordinate of joint between links 1 and 2, and y_D is the y-axis coordinate of joint D between links 4 and 5.



(a) Second unit is just unlocked/Second unit begins locking



(b) First unit begins unlocking and to form interlocking with second unit/
First unit is just locked and relieve interlocking with second unit



(c) First unit is just unlocked and interlocked with second unit/
First unit begins locking and to relieve the interlocking with second unit

Fig. 19. Several key stages while deploying/retracting.

Because $v_3 = v_C = \dot{y}_C$ and $v_4 = v_D = \dot{y}_D$, the velocity relationship between links 4 and 3 can be obtained by differentiating Eq. (20). The length of l_{14} determine the transform position from unlocking stage to retracting stage. The transform positions are shown in Fig. 14 while $l_{14} = 45.5 \text{ mm}$ & $l_{14} = 25.26 \text{ mm}$. Assuming unlocking velocity $v_D = -1 \text{ mm/s}$, the curves of the displacement, velocity and acceleration of link 3 are shown in Figs. 15–17, respectively. In the figures curve 1 shows the variation of link 3 for $l_{14} = 25.26 \text{ mm}$, curve 2 shows the variation of link 3 for $l_{14} = 45.5 \text{ mm}$. When $l_{14} = 25.26 \text{ mm}$, the curves are smooth until the velocity of link 3 achieves -1 mm/s . When $l_{14} = 45.5 \text{ mm}$, the velocity suddenly changes at the transform position as shown in Fig. 16, and the acceleration increases sharply and then reduces to 0 in short time as shown in Fig. 17.

The transformation between different stages of the metamorphic cell must be smooth and with less impact. During transition from deploying stage to locking stage or the transition from unlocking stage to retracting stage, the velocity of link 3 is expected to be identical to the velocity of link 4. According to Eq. (19), if $v_D = v_C$, there must be

$$\sin \varphi (\tan \phi + \tan \gamma) = 0 \tag{23}$$

This means $\varphi = 0$ or $\phi + \gamma = 0$.

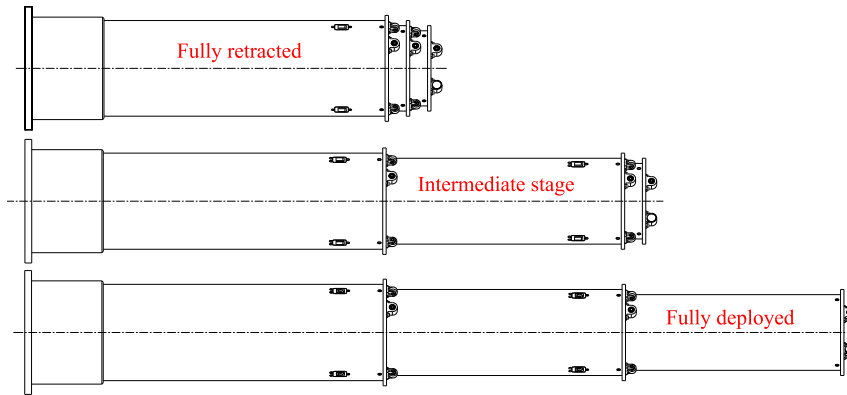


Fig. 20. Display of the whole system.

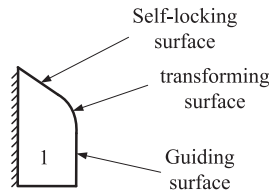


Fig. 21. Modified surface of body 1.

When $\phi + \gamma = 0$, the metamorphic mechanism cell is in singular state, as shown in Fig. 14.

When $\varphi = 0$, the orientation angle of part 1 must gradually changes to 0° from one specific nonzero value. This can be used to guide the design of actual prototype.

6.2. Implement design

Using this design method, a straight line deployable mechanism is built. Each unit has 3 metamorphic cells and the whole mechanism has 2 orders. This deployable/retracted mechanism is driven by cables. Because in deploying/retracting process the mechanism has only 1 DoF, one driver is used in this model. The cable drive system is shown in Fig. 18(a). The orderly deployable/retractable mechanism system is shown in Figs. 18(b) and (c).

This mechanism consists of 3 concentric cylindrical tubes and 2 metamorphic units with 3 metamorphic cells radially symmetrically distributed. The cable drum which winds the deployment and retraction cables is driven by one motor. Two cables routed symmetrically are used to deploy the system. One retraction cable is fixed on the rear of the smallest tube in accordance with the central axis of the tube to retract the system. The diameters of the tubes are in a descending order. The smaller tube can straight slide along the inside wall of the larger one. When the system is fully deployed the adjacent tubes are locked as shown in Fig. 18(c). When the system is fully retracted the adjacent tubes are interlocked except the first tube and second tube as shown in Fig. 18(b). The tubes of the system can be deployed/retracted sequentially. In deploying process, the deploying order is from tube 2 to tube 3. In retracting process, the retracting order is from tube 3 to tube 2. Some key stages of deploying/retracting are listed in Fig. 19. Sequence, 18(c)–19(a)–19(b)–19(c)–18(b), demonstrates the retracting process of the whole system. Sequence 18(b)–19(c)–19(b)–19(a)–18(c) demonstrates the deploying process. Fig. 20 shows the display of the system in different stages.

In order to reduce the influence of transformation impact, the housing of body 1 is designed with 3 sections as shown in Fig. 21. Self-locking section is plane surface, transforming section is cylinder surface and guiding surface is plane surface. A model in ADAMS was built to simulate the unlocking process of the model as shown in Fig. 22. The third tube unlocking stage was simulated. While unlocking velocity $v_D = -1\text{mm/s}$, displacement, velocity and acceleration of tube 3 are shown in Figs. 23–25, respectively. All curves are smooth, and transformation impact is eliminated in unlocking process by the specific design.

7. Conclusions

A metamorphic mechanism cell was designed to construct multistage orderly deployable/retractable mechanism using friction effect and driving condition. This cell can realize self-locking, unlocking and inter-locking with other cells. The friction self-locking and unlocking conditions were analyzed to determine the parameters of the cell, and self-locking margin was proposed to estimate the self-locking capability. Parallel and serial extensions of the cells were represented and mul-

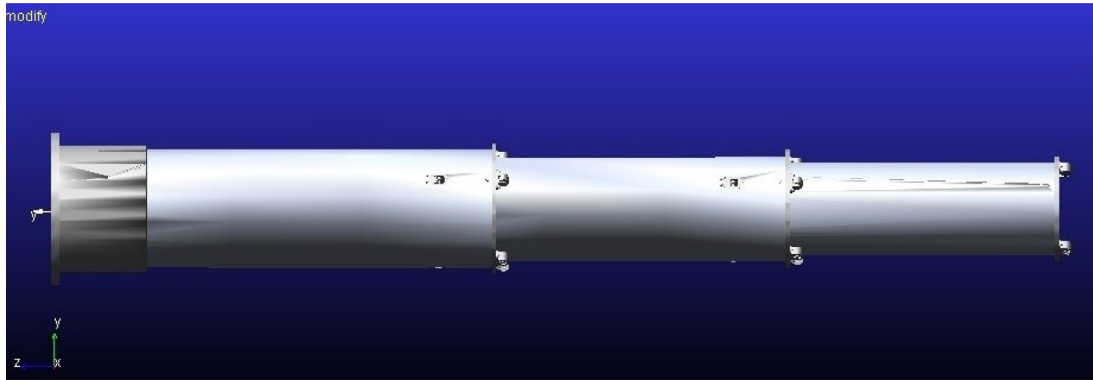


Fig. 22. Model in ADAMS.

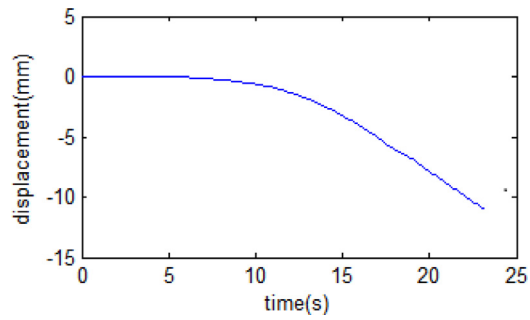


Fig. 23. Displacement of tube 3 when unlocking and retracting.

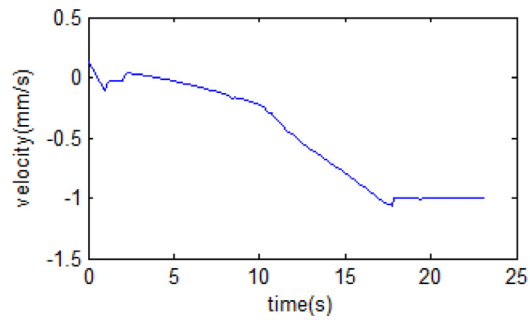


Fig. 24. Velocity of tube 3 when unlocking and retracting.

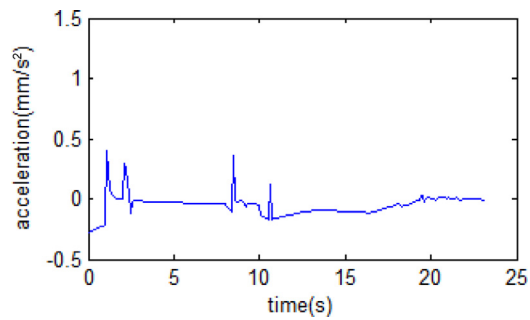


Fig. 25. Acceleration of tube 3 when unlocking and retracting.

tistage orderly deployable/retractable mechanisms could be constructed by these extensions. A model of one orderly deployable/retractable mechanism was developed with cable-pulley driving system. The design method was verified with the unlocking simulation tests. Transformation impact was mitigated by specific design of the self-locking surface.

Acknowledgment

The financial supports from [National Natural Science Foundation of China](#) (Grant No. 51305009), National Natural Science Foundation of China Key Program (Grant No. 51635002), State Key Laboratory of Robotics and System (HIT) and China scholarship council are gratefully acknowledged.

References

- [1] J.S. Dai, J.R. Jones, Mobility in metamorphic mechanisms of foldable/erectable kinds, *J. Mech. Des.* 121 (3) (1999) 375–382.
- [2] H.S. Yan, N.T. Liu, Finite-state-machine representations for mechanisms and chains with variable topologies, in: *Proceedings of the 26th ASME Mechanisms Conference*, Sept, Baltimore, Maryland, 2000, pp. 10–13.
- [3] N.T. Liu, *Configuration Synthesis of Mechanisms With Variable Chains*, Ph.D. dissertation, Department of Mechanical Engineering, National Cheng Kung University, Tainan, Taiwan.
- [4] H.S. Yan, C.H. Kuo, Topological representations and characteristics of variable kinematic joints, *J. Mech. Des.* 128 (2) (2006) 384–391.
- [5] H.S. Yan, C.H. Kuo, Structural analysis and configuration synthesis of mechanisms with variable topologies, in: *ASME/IFTOMM International Conference on Reconfigurable Mechanisms and Robots*, 2009, pp. 23–31.
- [6] D. Gan, J.S. Dai, Q. Liao, Mobility change in two types of metamorphic parallel mechanisms, *J. Mech. Robot* 1 (4) (2009) 041007.
- [7] J.S. Dai, J.R. Jones, Matrix representation of topological changes in metamorphic mechanisms, *J. Mech. Des.* 127 (4) (2005) 837–840.
- [8] D. Li, Z. Zhang, J.M. McCarthy, A constraint graph representation of metamorphic linkages, *Mech. Mach. Theory* 46 (2) (2011) 228–238.
- [9] X. Ding, Y. Yang, J.S. Dai, Topology and kinematic analysis of color-changing ball, *Mech. Mach. Theory* 46 (1) (2011) 67–81.
- [10] D. Li, Z. Zhang, J.M. McCarthy, A constraint graph representation of metamorphic linkages, *Mech. Mach. Theory* 46 (2) (2011) 228–238.
- [11] M.A. Pucheta, A. Butti, V. Tamellini, et al., Topological synthesis of planar metamorphic mechanisms for low-voltage circuit breakers, *Mech. Des. Struct. Mach.* 40 (4) (2012) 453–468.
- [12] S. Li, J.S. Dai, Structure synthesis of single-driven metamorphic mechanisms based on the augmented Assur groups, *J. Mech. Robot* 4 (3) (2012) 385–390.
- [13] S.S. Balli, S. Chand, Five-bar motion and path generators with variable topology for motion between extreme positions, *Mech. Mach. Theory* 37 (11) (2002) 1435–1445.
- [14] S.S. Balli, S. Chand, Synthesis of a planar seven-link mechanism with variable topology for motion between two dead-center positions, *Mech. Mach. Theory* 38 (11) (2003) 1271–1287.
- [15] A.A. Oledzki, Modeling and simulation of self-locking drives, *Mech. Mach. Theory* 30 (6) (1995) 929–942.
- [16] M. Leonasio, G. Bianchi, Self-locking analysis in closed kinematic chains, *Mech. Mach. Theory* 44 (11) (2009) 2038–2052.
- [17] K. Xu, X. Ding, Typical gait analysis of a six-legged robot in the context of metamorphic mechanism theory, *Chin. J. Mech. Eng.* 26 (4) (2013) 771–783.
- [18] K. Xu, X. Ding, Gait analysis of a radial symmetrical hexapod robot based on parallel mechanisms, *Chin. J. Mech. Eng.* 27 (5) (2014) 867–879.
- [19] X. Ding, X. Li, Design of a type of deployable/retractable mechanism using friction self-locking joint units, *Mech. Mach. Theory* 92 (2015) 273–288.
- [20] N.F. Knight, K.B. Elliott, J.D. Templeton, et al., FAST mast structural response to axial loading: modeling and verification, 53rd AIAA/ASME/ASCE/AHS/ASC structures, Structural Dynamics and Materials Conference 20th AIAA/ASME/AHS Adaptive Structures Conference 14th AIAA, 2012, 1952.
- [21] K.N. Schrader, R.H. Fetner, S.F. Griffin, et al., Development of a sparse-aperture testbed for optomechanical control of space-deployable structures, in: *Astronomical Telescopes and Instrumentation*, International Society for Optics and Photonics, 2002, pp. 384–395.
- [22] M. Schmid, M. Aguirre, Extendable retractable telescopic mast for deployable structures, 20th Aerospace Mechanisms Symposium, 1986.
- [23] M. Humphries, A. Haslehurst, D. Forster, The design and development of amulti element telescopic Boom (known as the Sula Boom), 12th European Space Mechanisms and Tribology Symposium (ESMATS), September 19, 2007–September 21, 2007, European Space Agency, 2007.
- [24] M. Leipold, H. Runge, C. Sickinger, Large SAR membrane antennas with lightweight deployable booms, 28th ESA AntennaWorkshop on Space Antenna Systems and Technologies, 8, European Space and Technology Research Centre, 2005.
- [25] J. Cai, X. Deng, J. Feng, Y. Xu, Mobility analysis of generalized angulated scissor-like elements with the reciprocal screw theory, *Mech. Mach. Theory* 82 (2014) 256–265.
- [26] J. Cai, Y. Xu, J. Feng, Kinematic analysis of Hoberman's linkages with the screw theory, *Mech. Mach. Theory* 63 (2013) 28–34.